Quantitative Analysis of Synaptic Phosphorylation and Protein Expression*[S]

Jonathan C. Trinidad‡, Agnes Thalhammer§, Christian G. Specht§¶, Aenoch J. Lynn‡, Peter R. Baker‡, Ralf Schoepfer§‖, and Alma L. Burlingame‡**

The postsynaptic density (PSD) signaling machinery contains proteins with diverse functions. Brain region-specific variations in PSD components mediate distinct physiological responses to synaptic activation. We have developed mass spectrometry-based methods to comprehensively compare both relative protein expression and phosphorylation status from proteins present in biochemical preparations of postsynaptic density. Using these methods, we determined the relative expression of 2159 proteins and 1564 phosphorylation sites in PSD preparations from murine cortex, midbrain, cerebellum, and hippocampus. These experiments were conducted twice using independent biological replicates, which allowed us to assess the experimental and biological variability in this system. Concerning protein expression, cluster analysis revealed that known functionally associated proteins display coordinated synaptic expression. Therefore, proteins identified as co-clustering with known protein complexes are prime candidates for assignment as previously unrecognized components. Concerning degree of phosphorylation, we observed more extensive phosphorylation sites on *N*-methyl-D-aspartate (NMDA) receptors than α-amino-3-hydroxy-5-methyl-4-isoxazolepropionic acid (AMPA) receptors, consistent with the central role of *N*-methyl-D-aspartate receptors in processing synaptic transmission patterns. Average kinase and phosphatase levels were highest in the hippocampus, correlating with a higher overall phosphopeptide abundance present in this brain region. These findings suggest that the hippocampus utilizes reversible protein phosphorylation to a greater extent than other brain regions when modifying synaptic strength. ***Molecular & Cellular Proteomics 7:684–696, 2008.***

Synaptic transmission between neurons in the central nervous system involves the release of neurotransmitter from presynaptic neurons and its detection by specific ligand-gated ion channels in the surface membrane of postsynaptic neurons. These neurotransmitter receptors exist as part of a highly organized protein complex known as the postsynaptic density (PSD).[1] In addition to neurotransmitter receptors, the PSD is composed of proteins of diverse function (1, 2). These functional groups include scaffolding molecules, kinases and phosphatases, G proteins and their effectors, and adhesion proteins.

The coordinated functioning of the different PSD components regulates in part the strength of signaling between the pre- and postsynaptic neurons. At the molecular level, this regulation can be achieved by alterations in protein localization (3–5), reversible post-translational modifications (*e.g.* phosphorylation (6, 7) and *O*-GlcNAc glycosylation (8)), and changes in protein levels via local synthesis and degradation (9). Integration of these processes may be the basis of long term changes in synaptic efficacy thought to underlie higher cognitive processes such as learning and memory (10).

Proteomics approaches aimed at identifying synaptic proteins (11–16) and their post-translational modifications (8, 17, 18) have increased our knowledge of synaptic complexity. However, it is difficult to assign biological function to individual proteins/phosphorylation sites based only on their identification in a proteomics study. To gain insights into the role of specific proteins and phosphorylation sites, it is important to understand how their synaptic levels vary with changes of physiological and pharmacological conditions as well as in diseases affecting the central nervous system. One recent study examined the relative expression of synaptic proteins in two brain regions, and absolute quantification was conducted on a small subset of proteins (19). A second study has examined phosphorylation in synaptosomes and focused on quantitative changes in a limited subset of sites (20). Quantification using mass spectrometry can be performed using isotopic labeling or label-free methods (21).

In the present study, we isolated PSD complexes from the cortex, midbrain, cerebellum, and hippocampus and used the iTRAQ multiplexed chemical labeling reagent with tandem MS

From the ‡Mass Spectrometry Facility, Department of Pharmaceutical Chemistry, University of California, San Francisco, California 94143 and §Laboratory for Molecular Pharmacology, Department of Pharmacology, University College London, Gower Street, London WC1E 6BT, United Kingdom

Received, April 13, 2007, and in revised form, November 29, 2007
Published, MCP Papers in Press, December 3, 2007, DOI 10.1074/mcp.M700170-MCP200

[1] The abbreviations used are: PSD, postsynaptic density; CaMKII, calcium/calmodulin-dependent protein kinase II; GluR, ionotropic glutamate receptor; NMDA, *N*-methyl-D-aspartate; SCX, strong cation exchange; SOM, self-organizing map; AMPA, α-amino-3-hydroxy-5-methyl-4-isoxazolepropionic acid; TARP, transmembrane AMPA receptor regulatory protein; iTRAQ, isobaric tagging for relative and absolute quantitation; MINT, Molecular INTeraction; Qq-Tof, quadrupole selecting, quadrupole collision cell, time-of-flight.

(22) to obtain comparative protein abundance ratios on 2159 unique proteins and 1564 unique sites of phosphorylation. We show that a subset of annotated protein-protein interactions displayed highly correlated expression suggesting that these new highly correlating protein pairs are candidates for novel protein-protein interactions. We found large differences in the number of sites utilized at various levels of phosphorylation of NMDA receptors relative to AMPA receptors. Finally we demonstrated that proteins involved in kinase signaling have a higher overall abundance in the hippocampus and that their average phosphorylation stoichiometry is significantly higher there than in other brain regions.

EXPERIMENTAL PROCEDURES

PSD Sample Preparation and Quality Control—The entire quantification experiment was conducted twice using two sets of PSD samples that were independently purified at 4 °C as described previously (15). Briefly brains from adult mice (strain C57BL/6J; first experiment: 3–12 months of age; second experiment: 4–16 months; $n \geq 14$ per experiment) were dissected; the cerebellum (excluding brainstem) was first removed followed by the cortical hemispheres (excluding olfactory bulbs). The intermediate brain regions were referred to as "midbrain." The hippocampal formation was dissected from the cortex. The duration of the entire dissection was below 5 min. Brain regions (cerebellum, cortex, hippocampus, and midbrain) were immediately frozen in liquid nitrogen, and material from several animals was combined prior to the biochemical purification. The brain tissue was homogenized in a sucrose buffer containing a mixture of phosphatase inhibitors (1 mM Na_3VO_4, 1 mM NaF, 1 mM Na_2MoO_4, 4 mM sodium tartrate, 100 nM fenvalerate, 250 nM okadaic acid) and cleared by centrifugation. For each brain region, the ratio of buffer volume to starting brain weight was kept constant (10 ml of buffer/g) to ensure that each PSD prep was exposed to an equivalent level of phosphatase inhibitors. The membranous fraction was layered on a sucrose density and fractionated by centrifugation. Synaptic membranes were collected at the 1.0–1.2 M interface and applied onto a second gradient. The PSD fraction was collected at the 1.4–2.2 M interface and pelleted. Average yields of PSD sample per brain for individual regions were approximately as follows: 600 μg for cortex, 280 μg for midbrain regions, 190 μg for cerebellum, and 60 μg for hippocampus.

Digestion of PSD Samples—500 μg of each PSD sample were processed in parallel. Each PSD sample was resuspended in 25 mM ammonium bicarbonate containing 6 M guanidine hydrochloride. The mixture was incubated for 1 h at 57 °C with 2 mM tris(2-carboxyethyl)phosphine hydrochloride to reduce cysteine side chains; these side chains were then alkylated with 4.2 mM iodoacetamide in the dark for 45 min at 21 °C. The mixture was diluted 6-fold with 25 mM ammonium bicarbonate, and 5% (w/w) modified trypsin (Promega, Madison, WI) was added. The pH was adjusted to 8.0, and the mixture was digested for 12 h at 37 °C. The digests were desalted using a C_{18} Sep-Pak cartridge (Waters, Milford, MA) and lyophilized to dryness using a SpeedVac concentrator (Thermo Electron, San Jose, CA).

iTRAQ Labeling of Tryptic PSD Digests—The dried peptides were resuspended in 80 μl of iTRAQ dissolution buffer. Each iTRAQ reagent vial was reconstituted using 70 μl of ethanol, and a total of five reagent vials were used to label each 500-μg digest of tryptic peptides. For the first experiment, each set of iTRAQ reagents was combined with a specific brain region PSD digest as follows: the cortex with 114, the midbrain regions with 115, the cerebellum with 116, and the hippocampus with 117. In the second replicate of the experiment, the labeling of the brain regions was reversed. The labeling reaction was allowed to proceed for 1 h at 21 °C. An aliquot was then examined using a 1-h LC-MS/MS run and searched allowing iTRAQ as a variable modification to confirm that over 99% of all peptides identified showed complete iTRAQ labeling. A second aliquot containing a 1:1:1:1 mixture of the four labeled samples was then analyzed by LC-MS/MS to determine whether any correction for protein amount needed to be made during the final combination of the four samples.

Strong Cation Exchange Chromatography—SCX chromatography was performed using an ÁKTA Purifier (GE Healthcare) equipped with a Tricorn 5/200 column (GE Healthcare) packed in house with 5-μm 300-Å polysulfoethyl A resin (Western Analytical, Lake Elsinore, CA). The 2.0-mg combined PSD sample was loaded onto the column in 30% acetonitrile, 5 mM KH_2PO_4, pH 2.7 (buffer A). Buffer B consisted of buffer A with 350 mM KCl. The gradient went from 1% B to 29% B over 19 ml, from 29% B to 75% B over 14 ml, and from 75% B to 100% B over 2.5 ml. Between 90 and 100 fractions were collected and desalted using a MAX-RP reverse phase C_{18} cartridge (Phenomenex, Torrance, CA) and dried down using a SpeedVac concentrator. 5% of each fraction was reserved for analysis using ESI-Qq-TOF tandem MS, and the remaining 95% was subjected to titanium dioxide enrichment.

Enrichment of Phosphorylated Peptides Using Titanium Dioxide—Titanium dioxide enrichment was conducted on the remainder of each SCX fraction using an ÁKTA Purifier. Peptides were enriched using 5-μm titanium dioxide beads (GL Sciences, Tokyo, Japan) (23, 24) packed into an analytical guard column with a 62-μl packing volume (Upchurch Scientific, Oak Harbor, WA). Dried peptide pellets from individual SCX fractions were resuspended in 250 μl of wash solution (35% acetonitrile, 200 mM NaCl, 0.3% TFA) and run over the titanium dioxide column with an additional 3.9 ml of wash solution to remove non-phosphorylated peptides. This was then followed by 3.5 ml of rinse solution (5% acetonitrile, 0.1% TFA). Phosphorylated peptides were eluted from the titanium dioxide column directly onto a C_{18} macrotrap peptide column (Michrom Bioresources, Auburn, CA) using 15 ml of elution solution (1 M KH_2PO_4). The C_{18} column was then washed with 17.1 ml of rinse solution. Peptides were eluted from the C_{18} column using 400 μl of organic elution solution (50% acetonitrile, 0.1% TFA), and this solution was lyophilized to dryness using a SpeedVac concentrator.

Nano-LC-ESI-Qq-TOF Tandem Mass Spectrometry Analysis—Individual SCX and SCX-titanium dioxide fractions were separated using a 75-μm × 15-cm reverse phase C_{18} column (LC Packings, Sunnyvale, CA) at a flow rate of 350 nl/min, running a 3–32% acetonitrile gradient in 0.1% formic acid on an Agilent 1100 series HPLC system equipped with an autosampler (Agilent Technologies, Palo Alto, CA). Gradient cycle times were between 1.0 and 1.5 h in length depending on sample complexity. The LC eluent was coupled to a micro-ion spray source attached to a QSTAR Pulsar mass spectrometer (Applied Biosystems, Foster City, CA). Peptides were analyzed in positive ion mode. MS spectra were acquired for 1 s. For each MS spectrum, the two most intense multiple charged peaks were selected for generation of subsequent collision-induced dissociation MS. For precursor ion selection, the quadrupole resolution was set to "low," which allows for transmission of ions within ~2 *m/z* units of the monoisotopic mass. The collision-induced dissociation energy was automatically adjusted based upon peptide charge and *m/z* ratio. A dynamic exclusion window was applied that prevented the same *m/z* from being selected for 3 min after its initial acquisition.

Interpretation of MS/MS Spectra—Data were analyzed using Analyst QS software (version 1.1), and MS/MS centroid peak lists were generated using the Mascot.dll script (version 1.6b18). The MS/MS spectra were searched against the entire UniProt *Mus musculus* database (downloaded April 19, 2007 with a total of 64,717 entries) using the following parameters. Initial peptide tolerances in MS and

MS/MS modes were 200 ppm and 0.2 daltons, respectively. Trypsin was designated as the enzyme, and up to two missed cleavages were allowed. Carbamidomethylation and iTRAQ labeling of lysine residues were searched as fixed modifications. The peptide amino termini were fixed as either iTRAQ-modified or protein N-terminal acetylated. Oxidation of methionine was allowed as a variable modification. Phosphorylation of serine/threonine/tyrosine residues were only allowed for titanium dioxide-enriched fractions. All high scoring peptide matches (expectation value <0.01) from individual LC-MS/MS runs were then used to internally recalibrate MS parent ion *m/z* values within that run. Recalibrated data files were then searched with a peptide tolerance in MS mode of 50 ppm. The output of both searches was combined into a single output file for identification purposes, and proteins were considered positively identified if they were identified with at least one peptide with a Protein Prospector peptide score ≥ 25 and a peptide expectation value ≤ 0.01. The false positive rates were estimated by conducting the search using a concatenated database containing the original UniProt database as well as a version of each original entry where the sequence has been randomized. Protein accession numbers were mapped onto the corresponding UniGene entries, and proteins were condensed to single proteins for quantification and identification purposes if they matched to the same UniGene entry. Peptides that corresponded to proteins from more than one UniGene entry were not used for quantification. This resulted in quantification of 2839 unique UniGene entries using 19,037 unique peptide sequences with an overall protein false positive rate of 0.14% (four false positive proteins) and a peptide false positive rate of 0.026% (five false positive peptides). Both replicates led to a total identification of 1738 phosphorylated peptides with a false positive rate of 0.12% (two false positive phosphopeptides).

Evaluation of Phosphopeptide MS/MS Spectra—All phosphopeptides were manually inspected to verify that the majority of high abundance peaks were y or b sequence ions or y $-$ H_2O/H_3PO_4 or b $-$ H_2O/H_3PO_4 ions when appropriate. Site assignments were done manually with the assistance of an in-house site assignment script.

Quantification of Protein Expression and Phosphorylation Levels—The raw MS data in *.wiff format were read directly using Protein Prospector (version 4.24.4). For each peptide MS/MS spectrum, the raw area of the peaks at *m/z* 114.1, 115.1, 116.1, and 117.1 (± 0.1 *m/z*) was determined. iTRAQ area measurements were adjusted using isotope correction values supplied by the vendor for these batches of the reagent. If multiple MS/MS spectra were collected for the same peptide at the same charge state, only the best scoring spectra was used for quantification. To calculate the relative percentage of a given peptide in each of the four samples, the area of that corresponding peak was divided by the average area for all four iTRAQ diagnostic ions in that MS/MS spectra. Relative protein expression values for each UniGene protein entry were the log-averaged value of all (non-phosphorylated) peptides matching to that entry. Relative phosphorylation stoichiometries were calculated by normalizing relative phosphorylation levels by corresponding relative protein levels. For quantification purposes, only MS/MS spectrum where the most intense iTRAQ peak was ≥ 25 counts were used (see "Results"). No outlier data points were removed.

Bioinformatics Analysis—Using the program GenePattern (25), protein expression patterns were analyzed across both biological replicates to generate self-organizing maps (SOMs) of protein expression clusters. Hierarchical clustering was carried out to cluster both proteins as well as brain regions using the program Gene Cluster (26). The relative expression data were $\log_2$-transformed, median-centered, and normalized by brain region and then median-centered and normalized by gene. For both the SOM and hierarchical clustering analyses, average-linkage clustering, uncentered correlation was used as the similarity metric. To benchmark the hierarchical clustering results in terms of their ability to cluster protein-protein interactors, we utilized known protein-protein interactions as annotated in the Molecular INTeraction (MINT) database (27). This database annotates known physical interaction between proteins (either direct or indirect). A list was generated of those protein pairs in the MINT database for which both entries were quantified in our study (a total of 409 unique proteins). The average-linkage correlation value was determined for all possible pairwise combinations of these 409 proteins. The results were then separated into two populations: literature-annotated interactions and all other interactions.

Statistical Analysis—All statistical analysis was conducted using the RGui program, freely available on the World Wide Web. Because the distributions of ratio values were not necessarily normally distributed, the non-parametric Mann-Whitney *U* test was generally used to evaluate specific hypotheses.

RESULTS

Acquisition and Evaluation of Quantitative Data—To compare the relative amounts of protein and phosphorylation across brain regions, we prepared PSD samples from microdissections of cerebellum, cortex, hippocampus, and midbrain. Each regional PSD preparation was digested with trypsin, and the resulting peptides were labeled with one of the four versions of the stable isotope iTRAQ reagent to allow for comparison of relative abundance levels (22). All four samples were combined, and a multidimensional separation approach was used to identify and quantify proteins and phosphorylation sites as described previously (15) and shown schematically in Fig. 1*A* and supplemental Fig. 1. The first replicate of the experiment led to quantification of the relative expression of 1225 unique proteins (from a total of 5993 peptide identifications) and 860 unique sites of phosphorylation across synapses from the four brain regions (supplemental Tables S1 and S2).

For data from the first experimental replicate, we examined the precision of peptide measurements by examining proteins for which we identified 10 or more peptides. Although peptides with a maximum iTRAQ peak area of less than 25 counts had an average percent error of 29%, those peptides with a maximum area of greater than 25 had an average percent error of less than 13% (Fig. 1*B*). An iTRAQ peak with an area of at least 25 was therefore accepted as a threshold value, and overall these peptides displayed an S.D. of 0.18 relative to their respective calculated protein averages (Fig. 1*C*). A variable number of peptides were identified and quantified per protein with 61% of the proteins identified by two or more peptides (Fig. 1*D*). To evaluate the precision of protein measurements within an experiment, we calculated the S.E. values for protein ratios for proteins quantified with two or more peptides (Fig. 1*E*). The median S.E. for this dataset (assuming proteins quantified with a single peptide have maximum S.E. values) was 0.187 (representing a median protein ratio error of less than 19%). This indicates that overall protein level quantification has a high level of precision.

Reproducibility of Protein and Phosphorylation Quantification—A second preparation of PSDs was purified and ana-

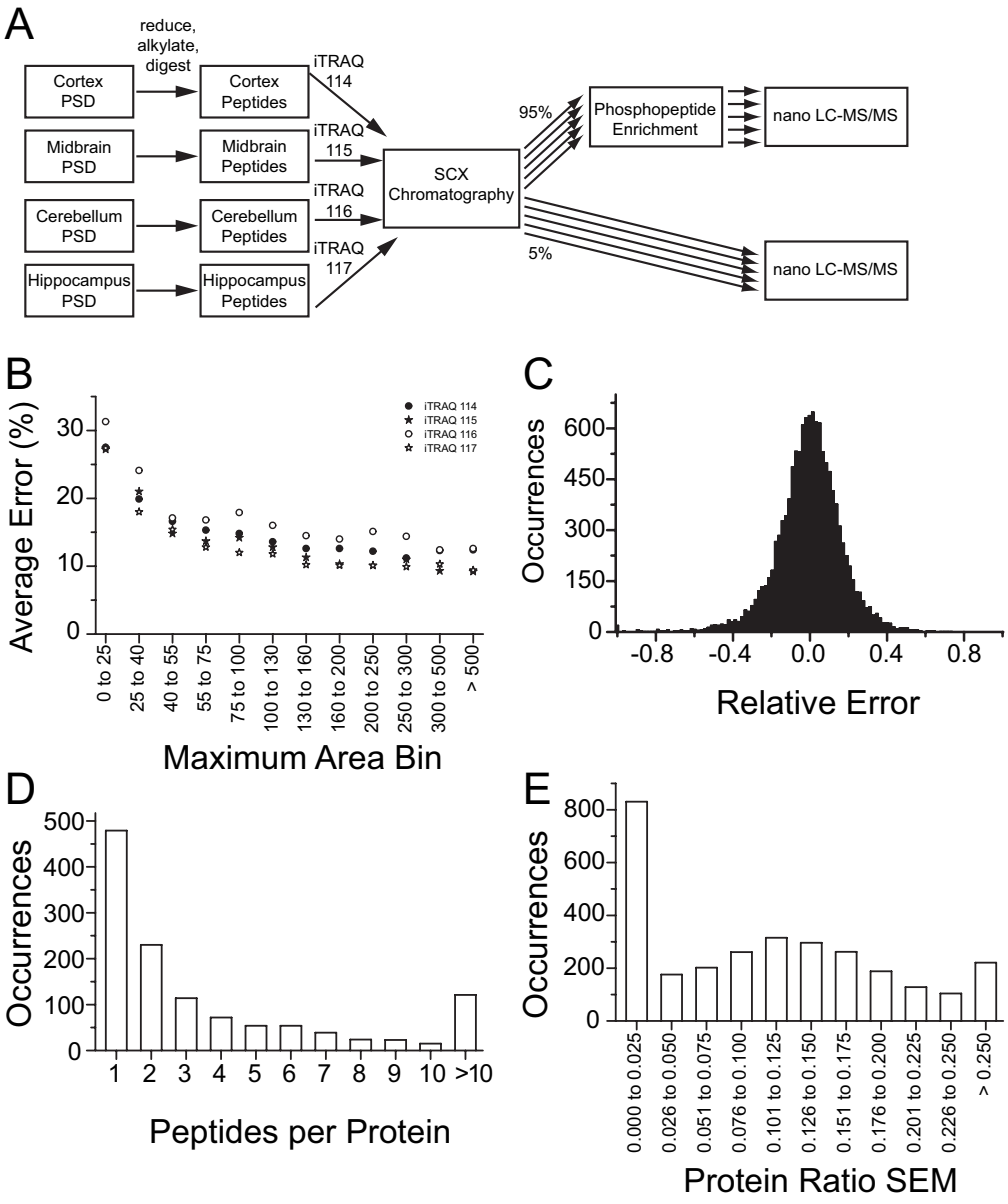

FIG. 1. **Assessment of quantification precision.** *A*, 500 μg of postsynaptic density proteins were purified from each of the following regions: cortex, midbrain regions, cerebellum, and hippocampus. The proteins were independently reduced, alkylated, and digested with trypsin and then labeled with individual versions of the iTRAQ reagent. The samples were then combined and subjected to strong cation exchange chromatography. Approximately 5% of each SCX fraction was subjected to LC-MS/MS to identify and quantify non-phosphorylated peptide (protein) expression. The remainder of each SCX fraction was enriched for phosphopeptides by passage over a titanium dioxide column. These fractions were then analyzed by LC-MS/MS. *B*, the absolute percent difference between individual peptide values and their respective protein values (normalized to the specific protein value) was calculated for all proteins with 10 or more unique peptides (136 proteins, 3158 total peptides, 12,632 total ratios). These data are shown as a histogram of the average percent error for bins corresponding to the area of the most abundant iTRAQ peak for each peptide, broken down by each iTRAQ label (*i.e.* brain region). The quantification for peptides with a maximum iTRAQ area below 25 counts had an average error from the calculated protein value of 29%, whereas those with an area above 25 counts had an average error of 13%. The specific error associated with each iTRAQ reagent was quite consistent with perhaps a slight increase for the 116 label. *C* is a histogram showing the relative error for the four iTRAQ peaks from each peptide in *B* that had a maximum area of greater than 25 counts (11,356 ratios from 2839 peptides). The S.D. of the relative error for peptide measurements compared with their respective protein values was 0.18. The data were plotted with a bin size of 0.0175. *D* is a histogram showing the number of peptides used to identify and quantify each protein. 746 proteins were quantified using two or more peptides. *E* shows the distribution of S.E. for each protein ratio measurement within a single experiment. A total of 2984 relative protein ratios were calculated (746 proteins $\times$ 4 iTRAQ ratios/protein). 479 proteins were quantified using a single peptide (resulting in 479 $\times$ 4 protein ratios), so S.E. values for these protein values were not determined. Assuming that proteins quantified with a single peptide had a maximal S.E., the median value for the entire dataset was 0.187. The median S.E. value for protein ratios from proteins quantified with more than one peptide was 0.102.

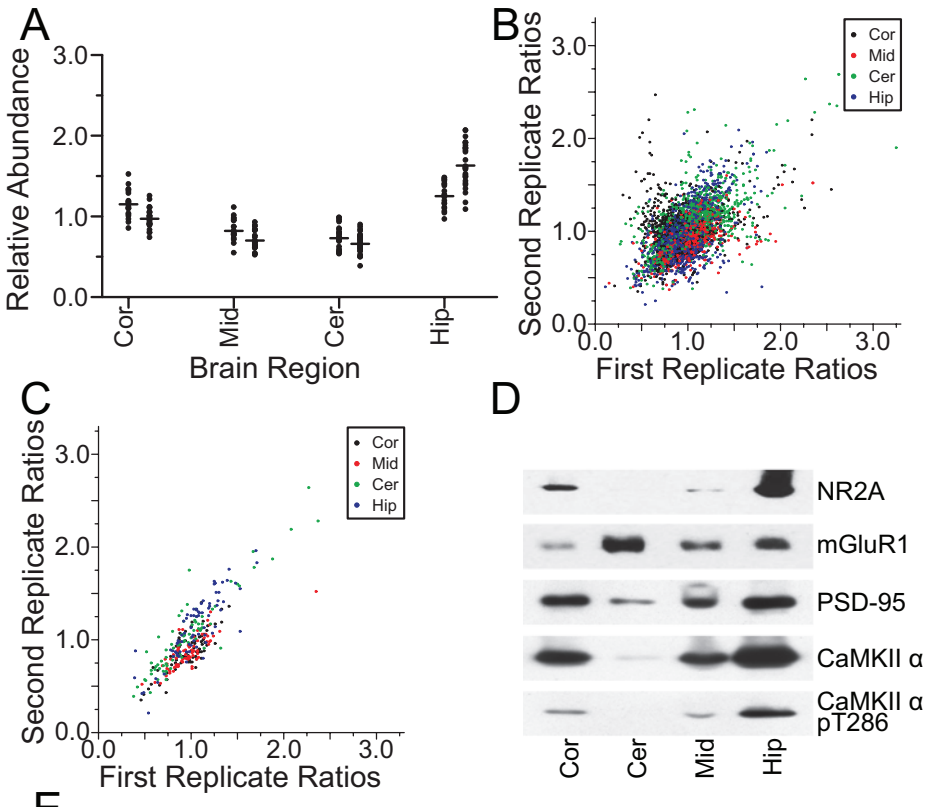

E

		Cor	Cer	Mid	Hip
1st replicate	CaMKII alpha protein	1.01	0.38	0.77	1.71
	phospho threonine 286	1.42	0.25	0.69	1.58
	relative stoichiometry	1.41	0.66	0.97	0.93
2nd replicate	CaMKII alpha protein	0.96	0.45	0.66	1.80
	phospho threonine 286	0.93	0.31	0.57	2.25
	relative stoichiometry	0.98	0.68	0.85	1.22
average	relative stoichiometry	1.19	0.67	0.91	1.08

FIG. 2. **Comparison of reproducibility across experimental replicates.** To determine the reproducibility of the data, we performed a second independent quantification experiment. *A* shows the ratio values for individual peptides (*single dots*) as well as the protein averages (*horizontal bars*) for the protein chapsyn-110 from the four brain regions. 21 and 29 unique chapsyn-110 peptides were identified in the first and second replicates, respectively. The two sets of data associated with each brain region represent both replicates of the experiment. *B* shows how well individual protein ratios agreed from the first replicate with the second. *Black*, cortex; *red*, midbrain regions; *green*, cerebellum; *blue*, hippocampus. *C* shows these data for only those proteins in *B* that were annotated as synaptic in the Gene Ontology database (a total of 77 proteins). *D*, Western blot comparison of PSD preparations from different brain regions illustrating regional abundance variations. PSD samples (10 μg/lane) were obtained from murine cortical ("*Cor*"), cerebellar ("*Cer*"), midbrain regions ("*Mid*"), and hippocampal ("*Hip*") material. *E*, a comparison of protein level and phosphorylation measurements across each brain region for calcium/calmodulin-dependent protein kinase IIα as measured by quantitative MS. The relative phosphopeptide expression ratios for each replicate were the average of the phosphopeptides QEtVDCLK and QEtVDCLKK (lowercase "t" designates the site of modification). These data allow for the calculation of relative stoichiometries of phosphorylation. *pT*, phosphothreonine.

lyzed to address the variance introduced by the PSD isolation procedure as well as from differences in the batches of mice used in the two independent experiments. This resulted in a total identification/quantification of 2024 proteins, 1090 of which were also identified in the first replicate (for a total of 2159 identified in either using a total of 16,242 peptide identifications). A total of 1564 unique sites of phosphorylation (1339 with intensities above the previously defined threshold) were quantified in at least one replicate. 637 of these phosphopeptides were quantified in both biological replicates (509 in both replicates with intensity above threshold at least once). A lower percentage of phosphorylation sites were quantified in both replicates (~41%) relative to the percentage of quantified proteins (~50%). This is largely due to the fact that it is easier to identify a given protein across replicates because proteins do not need to be identified using the same peptide(s) in each experiment. This is indicative of the fact that despite our enrichment further sites of phosphorylation remain to be identified, particularly those on low abundance proteins and/or of low stoichiometry.

To illustrate how peptide and protein measurements vary across replicates, we initially analyzed the values obtained at the level of a single protein, in this case chapsyn-110 (Fig. 2*A*). 26 and 28 non-phosphorylated peptides were identified in the replicates, and the relative order of protein abundance (hippocampus > cortex > midbrain ≈ cerebellum) was the same for both biological replicates.

For all proteins identified in both experiments, the median S.D. of protein ratios was 0.089, whereas the median S.D. for ratios of phosphopeptides identified in both experiments was 0.16. However, a number of proteins had ratios that varied considerably from one experiment to the next. A comparison of protein ratios in one experiment against those values in the second experiment showed a moderate degree of spread (Fig. 2*B*), and the r^2 value for the entire dataset was 0.26. Inspection of those proteins showing the poorest quantifica-

tion reproducibility revealed that many of them were cellular contaminants (*e.g.* histone proteins) whose presence would be expected to vary widely from preparation to preparation. As a rough guide to the quantification reproducibility of *bona fide* PSD components, we therefore selected those proteins annotated in the Gene Ontology as expressed at the synapse (28). Plotting this subset of proteins demonstrated that on a gross level our quantification of synaptic proteins was very reproducible with a median S.D. of 0.083 for these protein ratios and an r^2 value of 0.70 (Fig. 2*C*). As a further validation of our quantification method, we used Western blotting against several proteins and phosphothreonine 286 on CaMKIIα that all showed prominent region-specific expression (Fig. 2*D*). The rank order of expression levels thus obtained was consistent with our MS findings (supplemental Tables S1 and S2), further confirming the accuracy of our quantitative approach.

SOM Analysis of Protein Expression—Data obtained from microarray experiments have been used to demonstrated that gene expression clusters can be significantly enriched for genes of specific functional classes (29). To investigate how synapses from each brain region varied in their expression of protein functional classes, we used SOM analysis to group functional classes by their expression patterns. Proteins were organized at a general level to return five different maps (Fig. 3, *A–E).* Protein expression levels were generally consistent between both brain region replicates with the most notable exception being a cluster of proteins that had a low expression in the first cortical sample and higher expression in the second (Fig. 3*E*).

We examined how proteins of different functions were distributed among these SOM clusters by classifying each protein according to its Gene Ontology slim molecular function (GOTermMapper). Fig. 3, *F–Q*, shows the number of proteins annotated to specific protein functional classes. This analysis revealed a strong bias of kinases and phosphatases to be present in the SOM cluster showing highest expression in the hippocampus (SOM 0). Of the 87 proteins annotated as kinase(s) or phosphatase(s), 37% (32 proteins) mapped to SOM cluster 0. Overall only 25% (a total of 270) of the proteins grouped into SOM 0.

Hierarchical Clustering Analysis of Protein Expression—To investigate possible coordinated behavior of region-specific protein expression, we used average-linkage hierarchical clustering to group proteins on the basis of similarity of expression in each brain region (30, 31). The data were clustered both by brain regions and at the level of individual preparations (for a review of hierarchical clustering techniques, see Ref. 32). Fig. 4*A* shows these results for a subset of proteins with highest expression in the cerebellum. Consistent with the high level of reproducibility in the sample preparation and quantification (as shown in Fig. 2), individual brain region replicates were found to be the most similar to each other (see Fig. 4*A*, *top tree diagram*). This cerebellar enriched cluster contained Homer 3, glutamate receptor δ-2, inositol 3-phosphate receptor type 1, and mGluR4 (among others). A separate cluster is formed by proteins again with highest expression in the cerebellum but with a distinct expression pattern (Fig. 4*B*). Many of these proteins are ribosomal in nature. Although synapse-specific transcription does occur (for a review, see Ref. 33), this subset possibly represents contamination from cytosolic ribosomal pools. Proteins of unknown function whose expression profiles in the PSD preparations closely match known contaminants are themselves likely to be nonspecifically present in the sample. This approach is similar to that reported for the discrimination of contaminants in MS analyses of immunoprecipitates (34, 35).

Fig. 4*C* shows an example of a cluster of proteins with high hippocampal and low cerebellar expression, including the NMDA receptor subunit NR2B previously shown to be highly expressed in the hippocampus and cortex (36–38). Within each of the clusters represented in Fig. 4, *A–C*, were pairs of proteins annotated in the literature as physically interacting. Examples of this include Homer 3 with mGluR4 in Fig. 4*A*, the various ribosomal proteins in Fig. 4*B*, and NMDA receptor 1 with Discs large homolog 3 in Fig. 4*C*. The observation that specific pairs of physically interacting proteins were displaying correlated synaptic expression in our analysis suggested that as a more general rule protein-protein interactions might be observable by searching for correlated brain region-specific synaptic expression between proteins.

To evaluate this hypothesis, we used published protein-protein interactions annotated in the MINT database to benchmark the values obtained from the average-linkage hierarchical clustering analysis. The MINT database contained 629 pairwise interactions between 409 proteins quantified in our study. For each possible pairwise grouping of these 409 proteins (a total of $409 \times 408 \times 0.5$ pairs), we determined the closest hierarchical clustering node containing both entries and recorded their correlation value. These values were then separated into two groups based upon whether the protein pairs were annotated in the database as interacting. The overall distribution of correlations for literature-annotated interactions was significantly higher than the distribution of other protein pairs ($p < 8.88e{-}7$, Mann-Whitney *U* test). Literature-annotated pairs were 4.6 times more likely to have average-linkage correlation values greater than 0.90 (3.0 *versus* 0.64% for non-annotated pairs). Therefore, we conclude that protein pairs in our dataset that display highly correlated expression (although not being previously annotated as interacting) represent potential candidates for novel protein-protein interactors. Fig. 4*D* shows examples of protein pairs with high expression in various brain regions that display highly correlated expression (and were not annotated in the MINT database as interacting).

Analysis of Protein Phosphorylation—We identified 1564 unique phosphorylation sites on 831 proteins. In 61% of the cases, we were able to determine the exact amino acid phos-

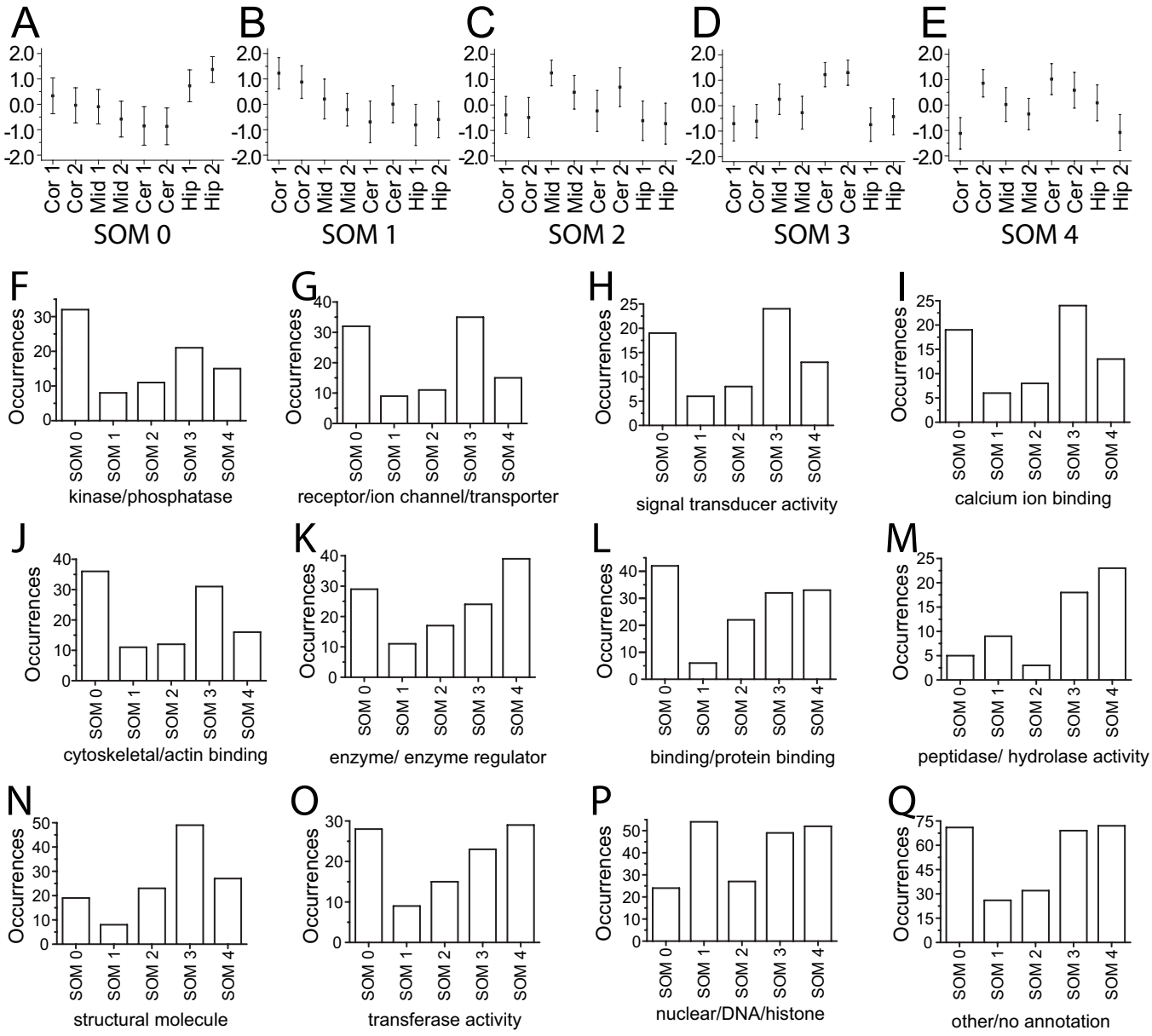

FIG. 3. **SOM analysis of protein expression.** *A–E*, results of self-organizing map analysis representing 270, 138, 153, 295, and 234 proteins, respectively. *Error bars* indicate the standard deviation of average expression. *F–Q*, for each protein in the previous self-organizing map clusters, we annotated the protein function using the Gene Ontology and grouped these function into 12 categories. For each category, we plotted the number of proteins that were present in each distinct SOM cluster. *Cor*, cortical; *Cer*, cerebellar; *Mid*, midbrain regions; *Hip*, hippocampal.

phorylated from the CID spectra. It is not always possible to determine the exact amino acid that is modified within a peptide. To positively identify a site of modification, a larger amount of spectral information is generally required relative to the amount needed to merely identify a MS/MS spectrum as matching to a specific phosphopeptide. If a given phosphopeptide contains more than one serine, threonine, or tyrosine, specific ions will need to be present in the MS/MS spectrum to distinguish among the possible modification sites. However, precise site assignment is important for eventual biological testing of specific sites. Three or more sites of phosphorylation were found on 167 proteins. Remarkably we identified only two phosphorylation sites between the four AMPA receptor subunits (see "Discussion").

Fig. 2*E* shows results from two experiments quantifying CaMKIIα protein expression and phosphorylation of threonine 286. In both replicates, relative phosphorylation was highest in the hippocampus followed by cortex, midbrain regions, and finally the cerebellum. This overall pattern was paralleled for protein expression. Dividing relative phosphorylation levels by

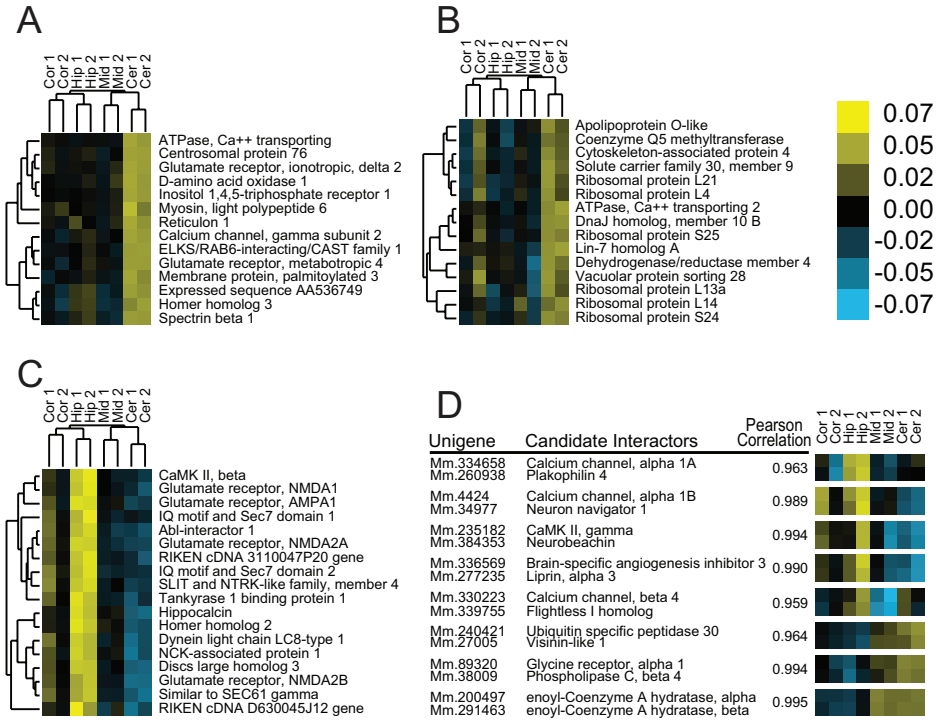

FIG. 4. **Average linkage hierarchical clustering reveals clusters of proteins with correlated expression.** *A* shows a cluster (correlation of 0.87) of synaptic proteins with highest expression in the cerebellum. The legend for *A–C* lists the numerical values of the relative expression ratios for the color scheme (after log transformation and centering and normalization of genes and arrays). *B* shows a second cluster (correlation of 0.78) of ribosomal proteins also with highest expression in the cerebellum. These two subclusters (*A* and *B*) were less well correlated (0.66) with each other. *C* shows a cluster (correlation of 0.93) of synaptic proteins with highest expression in the hippocampus. Proteins in this cluster showed 2.5–3-fold higher expression in the hippocampus relative to cerebellum. *D*, a candidate list of eight protein pairs whose protein expression is highly correlated across both replicates of the experiment but that were not reported as interacting in the MINT database. These pairs represent potential novel *in vivo* interactions (either physical or at the metabolic level). The final pair (enoyl-coenzyme A hydratase α and β) represents the two proteins in the entire dataset with the highest level of correlation and are known to interact (although they were not annotated in the MINT database). *Cor*, cortical; *Cer*, cerebellar; *Mid*, midbrain regions; *Hip*, hippocampal; *Mm*, Mus musculus; CAST, CAZ-associated structural protein.

the corresponding relative protein expression yields relative phosphorylation stoichiometries. This showed that although the level of threonine 286 phosphorylation was highest in the hippocampus it could be explained largely by the fact that protein expression was also highest in the hippocampus. Western blotting for CaMKIIα and phosphorylation of threonine 286 confirmed the trends observed by quantitative MS (Fig. 2*D*). In many biological comparisons (*e.g.* when comparing wild type *versus* diseased samples), changes in the amount of a given phosphorylation site (as measured, for example, by a phosphospecific antibody) can be due to either changes in protein level, changes in phosphorylation stoichiometry, or both. Our ability to determine the relative contribution from each of these factors enables us to investigate synaptic preparations on a level not obtainable by any other current methods.

In many cases, we quantified multiple phosphopeptides per protein. Fig. 5*A* shows the relative phosphorylation stoichiometries for 11 phosphorylated peptides from chapsyn-110. The largest change for the hippocampus relative to the cerebellum corresponded to serine 365, which had a >2-fold relative stoichiometry in the hippocampus relative to the cerebellum. The 11 phosphopeptides across both replicates showed a 25% higher average relative phosphorylation stoichiometry, when taken as a whole, in the hippocampus relative to the cerebellum ($n = 20$ total measurements, $p < 0.02$, Mann-Whitney *U* test).

To examine the overall distribution of phosphorylation and relative phosphorylation stoichiometry, we determined the relative stoichiometry for all phosphorylation sites in our dataset (supplemental Table S1). To directly compare any two brain regions, their relative stoichiometries can be expressed as a ratio. Table I lists the 10 sites displaying the greatest increase or decrease in relative phosphorylation stoichiometry between the hippocampus and cerebellum. Among sites showing highest relative stoichiometry in the hippocampus were two sites on densin 180 and two sites on liprin α3. In contrast, CaMKIIα showed four sites whose relative phosphorylation stoichiometries were 2-fold greater in the cerebellum than hippocampus (of a total of eight sites of phosphorylation).

Phosphorylation Status of Different Brain Regions—To address the overall regulation of phosphorylation across brain

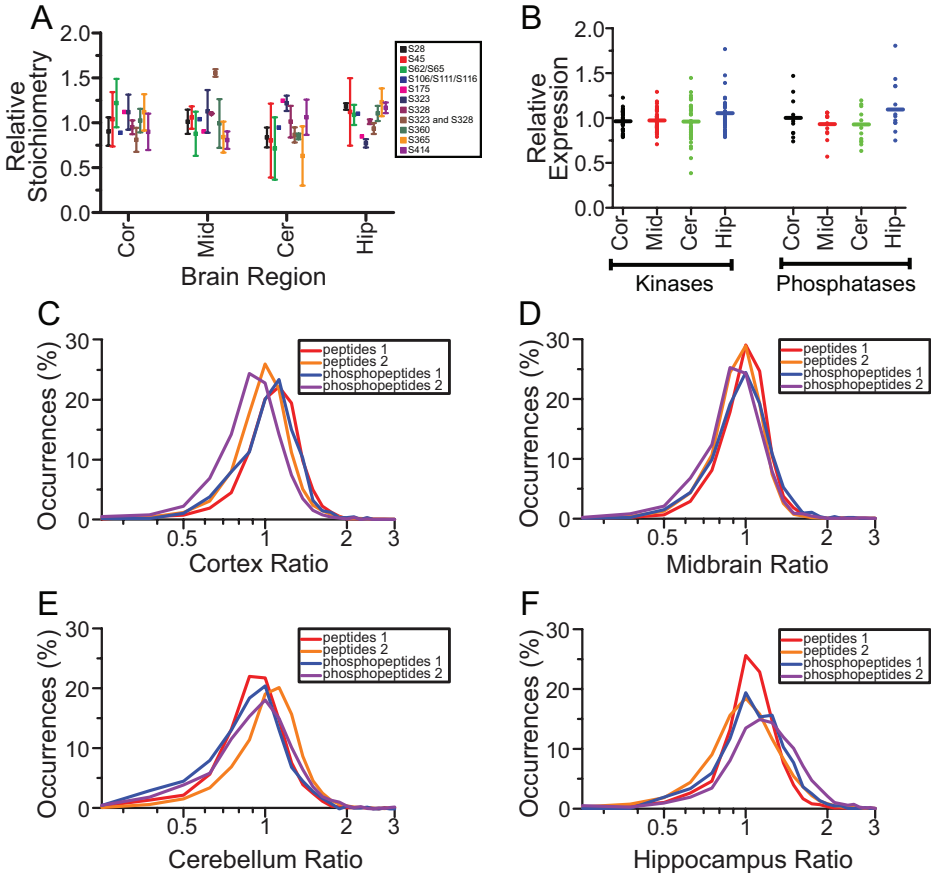

FIG. 5. **Analysis of regional phosphorylation.** *A* shows the relative phosphorylation stoichiometries for 11 phosphopeptides for chapsyn-110 across the four brain regions. To calculate relative phosphorylation stoichiometries, relative expression values for individual phosphopeptides were normalized by the protein expression for chapsyn-110. The legend lists the phosphorylated amino acid and its position within the protein. A *forward slash* indicates ambiguity regarding the site of phosphorylation. Plotted are the average and S.D. values for both replicates. In two cases (Ser-106/Ser-111/Ser-116 and Ser-175) a given phosphopeptide was only quantified in one replicate. In one instance (Ser-323 and Ser-328), a given phosphopeptide was doubly phosphorylated. *Solid squares* represent log-averaged mean values, and *error bars* represent the S.D. *B* shows the relative protein level ratios for proteins annotated as phosphatases (15 instances) and kinases (41 instances) and quantified in both biological replicates. *Single points* represent calculations of individual protein expression within a single experiment. *Colored bars* represent log-averaged values for the entire distribution. *C–F* show binned data (bin size of 0.125) from an examination of the distributions for non-phosphorylated and phosphorylated peptides from proteins found to be phosphorylated in this study. In the first replicate, 2716 non-phosphorylated and 693 phosphorylated peptides were quantified. In the second replicate, 10,246 non-phosphorylated and 1325 phosphorylated peptides were quantified. *Cor*, cortical; *Cer*, cerebellar; *Mid*, midbrain regions; *Hip*, hippocampal.

regions, we compared how phosphorylation levels varied with respect to protein expression for those proteins found to be phosphorylated. Fig. 5, *C–F*, shows the distribution of non-phosphorylated peptides and phosphorylated peptides across each of the brain regions. Treating each peptide measurement from both biological replicates as a unique measurement showed the hippocampus had a 13% increase in the overall relative expression of phosphorylated peptides compared with their non-phosphorylated counterparts ($p < 2.2e{-}16$, Mann-Whitney *U* test, $n = 12{,}962$ non-phosphorylated peptide measurements and 2018 phosphorylated peptide measurements). Fig. 5*B* shows the relative expression across brain regions of those proteins specifically annotated as having phosphatase or kinase function. Of those kinases identified with the most peptides (which is a rough measure of protein abundance), the CaMKII isoforms, and protein kinase Cγ showed highest expression in the hippocampus. In contrast, Doublecortin (39) and calcium/calmodulin-dependant protein kinase-like 1 (DCAMKL1) (40) showed highest expression in the cortex, and Citron Rho-interacting kinase (41) showed highest expression in the midbrain. Although expression of a given protein phosphatase or protein kinase does not necessarily correlate with its level of activity, the average expression of kinases and phosphatases were 9 and 15% higher in the hippocampus relative to other brain regions ($p < 8.8e{-}3$ and <0.026 for kinases and phosphatases, respectively, Mann-Whitney *U* test). This suggests that regulation of phosphorylation-based signaling plays a more prominent role in the hippocampus than in other brain regions.

TABLE I

Representative phosphorylation sites that display large changes in stoichiometry between the cerebellum and hippocampus

637 phosphorylated sites were quantified in both biological replicates. The table lists those sites showing a high, reproducible level of differential phosphorylation in the hippocampus relative to the cerebellum. The top portion of the table lists the 10 phosphorylation sites showing the highest hippocampus:cerbellum ratio; the bottom portion shows the 9 sites with the lowest ratio. Lowercase ″s, t, or y″ designates the site of modification. ″Acetyl-″ refers to protein amino terminal acetylation, and lowercase ″m″ refers to oxidation of methionine. Parentheses designate ambiguity regarding the exact site of modification. The relative stoichiometries in each brain region are listed along with the S.D. from both replicates in parentheses. The final column lists the ratio of relative phosphorylation in the hippocampus *versus* cerebellum. *Hip*, hippocampus; *Cer*, cerebellum.

Protein name	Peptide	Relative stoichiometry				
		Cortex	Midbrain	Cerebellum	Hippocampus	Hip/Cer
Densin 180	(sYstEsYGAsQtRPVsARPt)mAALLEK	0.75 (0.14)	0.60 (0.12)	0.25 (0.05)	1.55 (0.03)	6.22
Calcium channel α1E	FGEAVVVGRPGsGDGDSDQSR	1.31 (0.07)	0.87 (0.10)	0.48 (0.17)	1.46 (0.21)	3.06
Densin 180	SQsIDEIDVGTYK	0.83 (0.07)	0.83 (0.01)	0.49 (0.17)	1.31 (0.07)	2.67
Calcium channel γ3	DLsPISK	1.48 (0.61)	0.99 (0.08)	0.38 (0.20)	1.02 (0.33)	2.66
Liprin, α3	VSSSGLDsLGR	0.97 (0.14)	0.89 (0.03)	0.54 (0.08)	1.44 (0.03)	2.65
Amino acid transporter 4	Acetyl-(ss)HGNSLFLR	1.16 (0.23)	0.90 (0.39)	0.62 (0.22)	1.61 (0.39)	2.62
D15Wsu169e	FL(sLEYs)PVGK	0.48 (0.33)	0.64 (0.09)	0.66 (0.21)	1.61 (0.19)	2.46
CNK2	QEVTG(ssAVs)PIRK	1.01 (0.29)	0.61 (0.04)	0.60 (0.18)	1.41 (0.05)	2.36
Liprin, α3	sLPGSALELR	1.19 (0.16)	0.93 (0.20)	0.53 (0.07)	1.24 (0.01)	2.31
Munc13-1	ESYSDSmHsYEEFSEPR	0.96 (0.44)	0.88 (0.14)	0.59 (0.05)	1.34 (0.21)	2.29
GluR δ-2	APNGGFFRsPIK	0.80 (0.20)	0.86 (0.12)	1.16 (0.13)	0.58 (0.28)	0.50
Connexin 43	VAAGHELQPLAIVDQRP(ss)R	0.84 (0.33)	1.01 (0.03)	1.70 (0.41)	0.59 (0.26)	0.35
Ankyrin 3	RQsFASLALR	0.84 (0.08)	1.02 (0.29)	1.44 (0.12)	0.65 (0.29)	0.46
CaMKII, α	mLtINPSK	1.22 (0.02)	1.19 (0.12)	1.54 (0.24)	0.69 (0.05)	0.45
CaMKII, α	ITAAEALKHPWIsHR	1.14 (0.06)	1.28 (0.22)	1.57 (0.25)	0.69 (0.14)	0.44
CaMKII, α	LKGAILTtmLATR	0.99 (0.03)	1.14 (0.11)	2.44 (0.58)	0.64 (0.16)	0.26
CaMKII, α	AGAYDFPsPEWDTVTPEAK	1.06 (0.07)	1.58 (0.12)	1.57 (0.30)	0.63 (0.02)	0.40
Solute carrier family 12	EIQSI(tDEsRGs)IR	0.40 (0.02)	0.82 (0.13)	1.70 (0.00)	0.50 (0.16)	0.29
Diacylglycerol lipase, α	LLsPVAAASAAR	0.20 (0.11)	0.34 (0.12)	1.61 (0.14)	0.15 (0.04)	0.09

DISCUSSION

Information in the literature concerning specific protein expression has generally been focused on individual proteins present in a limited number of brain regions and on a selected small number of phosphorylation sites (19, 20). In contrast, this study has established the methodology required to allow for comprehensive identification and quantification of both protein expression and phosphorylation levels from complex mixtures such as postsynaptic densities. Label-free quantification can suffer from quantification artifacts when it is combined with multidimensional SCX fractionation because individual peptides can elute in more than one SCX fraction. In contrast, quantification using the iTRAQ strategy is not affected by SCX peak splitting as the signature iTRAQ reporter peaks still contain the full quantification information (as long as the their peak intensities remains above the threshold level). Furthermore the multiplexed nature of the iTRAQ reagent allows for a 4-fold decrease in the number of LC-MS/MS runs when compared with a label-free approach.

Here we provide relative quantification of 2159 proteins and 1564 sites of phosphorylation across synapses isolated from the cortex, midbrain regions, cerebellum, and hippocampus. The majority of proteins were identified and quantified with relatively high sequence coverage, leading to precise expression measurements (see "Results") that overall were extremely consistent with previously known expression patterns. For example, proteins known to be highly expressed in the cerebellum, including GluR2δ, mGluR1, mGluR4, inositol 3-phosphate receptor, the G-protein signaling regulator RGS8, Homer 3, and Munc13-3 (42–49), were observed among the 20 proteins with highest relative expression in the cerebellum.

Although our findings generally support results reported thus far in the literature, the extensive nature of our synaptic protein and phosphorylation quantification datasets allowed us to examine questions of synaptic biology from a global view compared with earlier, more traditional studies. For example, we demonstrated that proteins known to physically associate showed a high level of correlated expression and therefore suggest that those protein pairs correlating very highly in this dataset (that are not currently known to interact) represent potential novel protein-protein interactions. In addition, the ability to quantify the synaptic expression of 55 kinases and phosphatases and 1564 sites of phosphorylation allowed us to provide evidence for differential utilization of phosphorylation-based signaling by the hippocampus relative to other brain regions.

The individual brain regions analyzed in this study are far from homogeneous in their neuronal composition; they are known to be composed of several different types of neurons. Even within a given cell type, the range of molecularly distinct synaptic connections is expected to be very large. Although our approach does not allow differentiation between distinct sets of cell types or synaptic connections, it was still possible to observe evidence for protein-protein interactions by a region-to-region comparison of PSD components.

TABLE II
A list showing the Pearson correlation coefficients between the glutamate receptors AMPA 1–4 and other AMPA subunits as well as proteins reported to interact with AMPA receptors

	AMPA 1	AMPA 2	AMPA 3	AMPA 4
AMPA 2	0.94			
AMPA 3	−0.13	−0.13		
AMPA 4	−0.13	−0.13	0.57	
TARP γ-2	−0.13	−0.13	0.21	0.21
TARP γ-3	−0.13	−0.13	−0.03	−0.03
TARP γ-8	0.66	0.66	−0.13	−0.13

We observed that known protein interaction pairs displayed, on average, a high degree of correlated expression across brain regions. Nevertheless all of these literature-annotated interaction pairs did not have highly correlated expression. Several likely explanations exist for this observation. First, two proteins that directly interact will only show highly correlated synaptic expression if the majority of molecules of each protein are involved in forming these specific complexes. If instead a specific protein is associated with two distinct synaptic complexes, then its overall expression may not correlate well with any of the proteins in these two complexes. Second, it is unlikely that all protein pairs with literature-annotated interactions actually interact at synapses. In Fig. 4*D*, we listed eight pairs of proteins whose expression patterns were highly correlated, representing candidates for novel protein-protein interactions. These potential pairs represent proteins with increased expression in the various brain regions that to our knowledge have not been reported previously to interact.

To assemble a complete synaptic protein interaction network, it will be necessary to examine synapses using a series of orthogonal probes (*e.g.* excitatory stimulation and gene mutation studies) and to determine the ways in which protein expression and post-translational modification levels are coordinately regulated under unique biological phenotypes. The results of this current study are a first step toward that goal and have allowed us to examine specific protein groups in detail. This detailed analysis of protein groups both confirmed predictions from the literature and allowed for the formulation of new hypotheses that are discussed below.

One such group we examined included AMPA receptors and the transmembrane AMPA receptor regulator proteins (TARPs). TARPS are scaffolding molecules that play a role in the synaptic localization of AMPA receptors. AMPA receptors are tetramers composed of GluR subunits 1–4. We observed a high correlation between expression of GluR1 and GluR2, consistent with the notion that the GluR1/2 heterodimers are a predominant synaptic subtype (Table II). Of the TARPS quantified in our study, expression of TARP γ-8 was most highly correlated with GluR1 and GluR2. A high correlation also existed between TARP γ-2 (stargazin) and GluR4. This points to a differential association between GluR subtypes and specific members of the TARP family in line with γ-2- and γ-8-deficient mice showing impaired expression and function of these GluR subtypes (50–52).

Turning to the NMDA and AMPA receptor phosphorylation states, we detected comparable numbers of non-phosphorylated peptides for members of the NMDA receptor relative to the AMPA receptor family (71 *versus* 84 total non-phosphorylated peptides across both replicates, respectively). This would suggest that, taken as groups, NMDA and AMPA receptor subunits are present in roughly similar amounts in line with a recent report in the literature (19). However, we observed many more phosphorylated peptides for NMDA receptors (18) compared with AMPA receptors (2), consistent with the central role of NMDA receptors in detecting and processing synaptic transmission patterns.

Coordinated regulation of protein phosphorylation plays an important role in synaptic plasticity (53). To gain an overall perspective on region-specific differences in phosphorylation, we examined the distribution of phosphorylated peptides and non-phosphorylated peptides from proteins found to be phosphorylated in our study. This analysis demonstrated that the average level of phosphorylation was highest in the hippocampus. To investigate how this might occur molecularly, we compared protein expression of kinases and phosphatases across brain regions and found that the levels of both of these protein classes are highest in the hippocampus (Fig. 5*B*). Taken together, these findings indicate that the phosphorylation-based signaling is more active in the hippocampus, suggesting that these mechanisms play a more significant role in hippocampal synaptic plasticity than in other brain regions. During the activation of kinase signaling pathways, changes in phosphorylation stoichiometry at specific sites are typically stable on the order of minutes to a few days. The exact temporal dynamics result from competition between the specific kinases and phosphatases involved. Therefore, a larger role for phosphorylation-based signaling mechanisms in hippocampal synaptic plasticity could provide a cell biological explanation for the central role that the hippocampus plays in short term memory and its consolidation.

Here we present the first study quantitatively examining synaptic protein expression and phosphorylation on a large scale. Such an approach is crucial in identifying coordinated changes in synaptic composition and modification following changes in synaptic function by developmental regulation, pharmacological manipulations, and disease states that are unlikely to influence a single protein or site of phosphorylation in isolation.

Acknowledgment—We thank Craig Garner for suggestions on the manuscript.

* This work was supported by the Wellcome Trust and the Biotechnology and Biological Sciences Research Council (to R. S.) and by National Institutes of Health National Center for Research Resources Biomedical Research Technology Program Grants RR01614 and

RR14606 (to A. L. B.). The costs of publication of this article were defrayed in part by the payment of page charges. This article must therefore be hereby marked "*advertisement*" in accordance with 18 U.S.C. Section 1734 solely to indicate this fact.

S The on-line version of this article (available at http://www.mcponline.org) contains supplemental material.

¶ Present address: Biologie Cellulaire de la Synapse, U789, Ecole Normale Supérieure, Paris 75005, France.

‖ To whom correspondence may be addressed. E-mail: r.schoepfer@ucl.ac.uk.

** To whom correspondence may be addressed. E-mail: alb@cgl.ucsf.edu.

REFERENCES

1. Ziff, E. B. (1997) Enlightening the postsynaptic density. *Neuron* **19,** 1163–1174
2. Kennedy, M. B. (2000) Signal-processing machines at the postsynaptic density. *Science* **290,** 750–754
3. Malenka, R. C. (2003) Synaptic plasticity and AMPA receptor trafficking. *Ann. N. Y. Acad. Sci.* **1003,** 1–11
4. Colbran, R. J., and Brown, A. M. (2004) Calcium/calmodulin-dependent protein kinase II and synaptic plasticity. *Curr. Opin. Neurobiol.* **14,** 318–327
5. Smith, K. E., Gibson, E. S., and Dell'Acqua, M. L. (2006) cAMP-dependent protein kinase postsynaptic localization regulated by NMDA receptor activation through translocation of an protein kinase A anchoring protein scaffold protein. *J. Neurosci.* **26,** 2391–2402
6. Soderling, T. R., and Derkach, V. A. (2000) Postsynaptic protein phosphorylation and LTP. *Trends Neurosci.* **23,** 75–80
7. Yamauchi, T. (2002) Molecular constituents and phosphorylation-dependent regulation of the post-synaptic density. *Mass Spectrom. Rev.* **21,** 266–286
8. Vosseller, K., Trinidad, J. C., Chalkley, R. J., Specht, C. G., Thalhammer, A., Lynn, A. J., Snedecor, J. O., Guan, S., Medzihradszky, K. F., Maltby, D. A., Schoepfer, R., and Burlingame, A. L. (2006) O-Linked N-acetylglucosamine proteomics of postsynaptic density preparations using lectin weak affinity chromatography and mass spectrometry. *Mol. Cell. Proteomics* **5,** 923–934
9. Ehlers, M. D. (2003) Activity level controls postsynaptic composition and signaling via the ubiquitin-proteasome system. *Nat. Neurosci.* **6,** 231–242
10. Bliss, T. V., Collingridge, G. L., and Morris, R. G. (2003) Introduction. Long-term potentiation and structure of the issue. *Philos. Trans. R. Soc. Lond. B Biol. Sci.* **358**, 607–611
11. Li, K. W., Hornshaw, M. P., Van Der Schors, R. C., Watson, R., Tate, S., Casetta, B., Jimenez, C. R., Gouwenberg, Y., Gundelfinger, E. D., Smalla, K. H., and Smit, A. B. (2004) Proteomics analysis of rat brain postsynaptic density. Implications of the diverse protein functional groups for the integration of synaptic physiology. *J. Biol. Chem.* **279,** 987–1002
12. Peng, J., Kim, M. J., Cheng, D., Duong, D. M., Gygi, S. P., and Sheng, M. (2004) Semiquantitative proteomic analysis of rat forebrain postsynaptic density fractions by mass spectrometry. *J. Biol. Chem.* **279,** 21003–21011
13. Yoshimura, Y., Yamauchi, Y., Shinkawa, T., Taoka, M., Donai, H., Takahashi, N., Isobe T., and Yamauchi, T. (2004) Molecular constituents of the postsynaptic density fraction revealed by proteomic analysis using multidimensional liquid chromatography-tandem mass spectrometry. *J. Neurochem.* **88,** 759–768
14. Jordan, B. A., Fernholz, B. D., Boussac, M., Xu, C., Grigorean, G., Ziff, E. B., and Neubert, T. A. (2004) Identification and verification of novel rodent postsynaptic density proteins. *Mol. Cell. Proteomics* **3,** 857–871
15. Trinidad, J. C., Specht, C. G., Thalhammer, A., Schoepfer, R., and Burlingame, A. L. (2006) Comprehensive identification of phosphorylation sites in postsynaptic density preparations. *Mol. Cell. Proteomics* **5,** 914–922
16. Trinidad, J. C., Thalhammer, A., Specht, C. G., Schoepfer, R., and Burlingame, A. L. (2005) Phosphorylation state of postsynaptic density proteins. *J. Neurochem.* **92,** 1306–1316
17. Collins, M. O., Yu, L., Coba, M. P., Husi, H., Campuzano, I., Blackstock, W. P., Choudhary, J. S., and Grant, S. G. (2005) Proteomic analysis of in vivo phosphorylated synaptic proteins. *J. Biol. Chem.* **280,** 5972–5982
18. DeGiorgis, J. A., Jaffe, H., Moreira, J. E., Carlotti, C. G., Jr., Leite, J. P., Pant, H. C., and Dosemeci, A. (2005) Phosphoproteomic analysis of synaptosomes from human cerebral cortex. *J. Proteome Res.* **4,** 306–315
19. Cheng, D., Hoogenraad, C. C., Rush, J., Ramm, E., Schlager, M. A., Duong, D. M., Xu, P., Wijayawardana, S. R., Hanfelt, J., Nakagawa, T., Sheng, M., and Peng, J. (2006) Relative and absolute quantification of postsynaptic density proteome isolated from rat forebrain and cerebellum. *Mol. Cell. Proteomics* **5,** 1158–1170
20. Munton, R. P., Tweedie-Cullen, R., Livingstone-Zatchej, M., Weinandy, F., Waidelich, M., Longo, D., Gehrig, P., Potthast, F., Rutishauser, D., Gerrits, B., Panse, C., Schlapbach, R., and Mansuy, I. M. (2007) Qualitative and quantitative analyses of protein phosphorylation in naive and stimulated mouse synaptosomal preparations. *Mol. Cell. Proteomics* **6,** 283–293
21. Rinner, O., Mueller, L. N., Hubalek, M., Muller, M., Gstaiger, M., and Aebersold, R. (2007) An integrated mass spectrometric and computational framework for the analysis of protein interaction networks. *Nat. Biotechnol.* **25,** 345–352
22. Ross, P. L., Huang, Y. N., Marchese, J. N., Williamson, B., Parker, K., Hattan, S., Khainovski, N., Pillai, S., Dey, S., Daniels, S., Purkayastha, S., Juhasz, P., Martin, S., Bartlet-Jones, M., He, F., Jacobson, A., and Pappin, D. J. (2004) Multiplexed protein quantitation in Saccharomyces cerevisiae using amine-reactive isobaric tagging reagents. *Mol. Cell. Proteomics* **3,** 1154–1169
23. Pinkse, M. W., Uitto, P. M., Hilhorst, M. J., Ooms, B., and Heck, A. J. (2004) Selective isolation at the femtomole level of phosphopeptides from proteolytic digests using 2D-NanoLC-ESI-MS/MS and titanium oxide precolumns. *Anal. Chem.* **76,** 3935–3943
24. Larsen, M. R., Thingholm, T. E., Jensen, O. N., Roepstorff, P., and Jorgensen, T. J. (2005) Highly selective enrichment of phosphorylated peptides from peptide mixtures using titanium dioxide microcolumns. *Mol. Cell. Proteomics* **4,** 873–886
25. Reich, M., Liefeld, T., Gould, J., Lerner, J., Tamayo, P., and Mesirov, J. P. (2006) GenePattern 2.0. *Nat. Genet.* **38,** 500–501
26. Eisen, M. B., Spellman, P. T., Brown, P. O., and Botstein, D. (1998) Cluster analysis and display of genome-wide expression patterns. *Proc. Natl. Acad. Sci. U. S. A.* **95,** 14863–14868
27. Zanzoni, A., Montecchi-Palazzi, L., Quondam, M., Ausiello, G., Helmer-Citterich, M., and Cesareni, G. (2002) MINT: a Molecular INTeraction database. *FEBS Lett.* **513,** 135–140
28. Ashburner, M., Ball, C. A., Blake, J. A., Botstein, D., Butler, H., Cherry, J. M., Davis, A. P., Dolinski, K., Dwight, S. S., Eppig, J. T., Harris, M. A., Hill, D. P., Issel-Tarver, L., Kasarskis, A., Lewis, S., Matese, J. C., Richardson, J. E., Ringwald, M., Rubin, G. M., and Sherlock, G. (2000) Gene ontology: tool for the unification of biology. The Gene Ontology Consortium. *Nat. Genet.* **25,** 25–29
29. Tamayo, P., Slonim, D., Mesirov, J., Zhu, Q., Kitareewan, S., Dmitrovsky, E., Lander, E. S., and Golub, T. R. (1999) Interpreting patterns of gene expression with self-organizing maps: methods and application to hematopoietic differentiation. *Proc. Natl. Acad. Sci. U. S. A.* **96,** 2907–2912
30. Gibbons, F. D., and Roth, F. P. (2002) Judging the quality of gene expression-based clustering methods using gene annotation. *Genome Res*. **12,** 1574–1581
31. Handl, J., Knowles, J., and Kell, D. B. (2005) Computational cluster validation in post-genomic data analysis. *Bioinformatics* **21,** 3201–3212
32. Gollub, J., and Sherlock, G. (2006) Clustering microarray data. *Methods Enzymol.* **411,** 194–213
33. Pfeiffer, B. E., and Huber, K. M. (2006) Current advances in local protein synthesis and synaptic plasticity. *J. Neurosci.* **26,** 7147–7150
34. Tackett, A. J., DeGrasse, J. A., Sekedat, M. D., Oeffinger, M., Rout, M. P., and Chait, B. T. (2005) I-DIRT, a general method for distinguishing between specific and nonspecific protein interactions. *J. Proteome Res.* **4,** 1752–1756
35. Blagoev, B., Kratchmarova, I., Ong, S. E., Nielsen, M., Foster, L. J., and Mann, M. (2003) A proteomics strategy to elucidate functional protein-protein interactions applied to EGF signaling. *Nat. Biotechnol.* **21,** 315–318
36. Monyer, H., Sprengel, R., Schoepfer, R., Herb, A., Higuchi, M., Lomeli, H., Burnashev, N., Sakmann, B., and Seeburg, P. H. (1992) Heteromeric

NMDA receptors: molecular and functional distinction of subtypes. *Science* **256,** 1217–1221
37. Kutsuwada, T., Kashiwabuchi, N., Mori, H., Sakimura, K., Kushiya, E., Araki, K., Meguro, H., Masaki, H., Kumanishi, T., Arakawa, M., and Mishina, M. (1992) Molecular diversity of the NMDA receptor channel. *Nature* **358**, 36–41
38. Goebel, D. J., and Poosch, M. S. (1999) NMDA receptor subunit gene expression in the rat brain: a quantitative analysis of endogenous mRNA levels of NR1Com, NR2A, NR2B, NR2C, NR2D and NR3A. *Brain Res. Mol. Brain Res.* **69,** 164–170
39. Gleeson, J. G., Allen, K. M., Fox, J. W., Lamperti, E. D., Berkovic, S., Scheffer, I., Cooper, E. C., Dobyns, W. B., Minnerath, S. R., Ross, M. E., and Walsh, C. A. (1998) Doublecortin, a brain-specific gene mutated in human X-linked lissencephaly and double cortex syndrome, encodes a putative signaling protein. *Cell* **92,** 63–72
40. Lin, P. T., Gleeson, J. G., Corbo, J. C., Flanagan, L., and Walsh, C. A. (2000) DCAMKL1 encodes a protein kinase with homology to doublecortin that regulates microtubule polymerization. *J. Neurosci.* **20,** 9152–9161
41. Sarkisian, M. R., Rattan, S., D'Mello, S. R., and LoTurco, J. J. (1999) Characterization of seizures in the flathead rat: a new genetic model of epilepsy in early postnatal development. *Epilepsia* **40,** 394–400
42. Araki, K., Meguro, H., Kushiya, E., Takayama, C., Inoue, Y., and Mishina, M. (1993) Selective expression of the glutamate receptor channel δ2 subunit in cerebellar Purkinje cells. *Biochem. Biophys. Res. Commun.* **197,** 1267–1276
43. Catania, M. V., Landwehrmeyer, G. B., Testa, C. M., Standaert, D. G., Penney, J. B., Jr., and Young, A. B. (1994) Metabotropic glutamate receptors are differentially regulated during development. *Neuroscience* **61,** 481–495
44. Tanabe, Y., Nomura, A., Masu, M., Shigemoto, R., Mizuno, N., and Nakanishi, S. (1993) Signal transduction, pharmacological properties, and expression patterns of two rat metabotropic glutamate receptors, mGluR3 and mGluR4. *J. Neurosci.* **13,** 1372–1378
45. Lomeli, H., Sprengel, R., Laurie, D. J., Kohr, G., Herb, A., Seeburg, P. H., and Wisden, W. (1993) The rat δ-1 and δ-2 subunits extend the excitatory amino acid receptor family. *FEBS Lett.* **315,** 318–322
46. Maeda, N., Niinobe, M., Inoue, Y., and Mikoshiba, K. (1989) Developmental expression and intracellular location of P400 protein characteristic of Purkinje cells in the mouse cerebellum. *Dev. Biol.* **133,** 67–76
47. Gold, S. J., Ni, Y. G., Dohlman, H. G., and Nestler, E. J. (1997) Regulators of G-protein signaling (RGS) proteins: region-specific expression of nine subtypes in rat brain. *J. Neurosci.* **17,** 8024–8037
48. Shiraishi, Y., Mizutani, A., Yuasa, S., Mikoshiba, K., and Furuichi, T. (2004) Differential expression of Homer family proteins in the developing mouse brain. *J. Comp. Neurol.* **473,** 582–599
49. Augustin, I., Betz, A., Herrmann, C., Jo, T., and Brose, N. (1999) Differential expression of two novel Munc13 proteins in rat brain. *Biochem. J.* **337,** 363–371
50. Chen, L., Bao, S., Qiao, X., and Thompson, R. F. (1999) Impaired cerebellar synapse maturation in waggler, a mutant mouse with a disrupted neuronal calcium channel gamma subunit. *Proc. Natl. Acad. Sci. U. S. A.* **96,** 12132–12137
51. Hashimoto, K., Fukaya, M., Qiao, X., Sakimura, K., Watanabe, M., and Kano, M. (1999) Impairment of AMPA receptor function in cerebellar granule cells of ataxic mutant mouse stargazer. *J. Neurosci.* **19,** 6027–6036
52. Rouach, N., Byrd, K., Petralia, R. S., Elias, G. M., Adesnik, H., Tomita, S., Karimzadegan, S., Kealey, C., Bredt, D. S., and Nicoll, R. A. (2005) TARP γ-8 controls hippocampal AMPA receptor number, distribution and synaptic plasticity. *Nat. Neurosci.* **8,** 1525–1533
53. Lisman, J., Schulman, H., and Cline, H. (2002) The molecular basis of CaMKII function in synaptic and behavioral memory. *Nat. Rev. Neurosci.* **3,** 175–190